THE JOURNAL OF PHYSICAL CHEMISTRY C

ARTICLE

pubs.acs.org/JPCC

Three-Stage Growth of Glycine and Glycylglycine Nanofilms on Si(111)7×7 and Their Thermal Evolution in Ultrahigh Vacuum Condition: From Chemisorbed Adstructures to Transitional Adlayer to Zwitterionic Films

L. Zhang, A. Chatterjee, and K. T. Leung*

WATLab, and Department of Chemistry, University of Waterloo, Waterloo, Ontario N2L 3G1, Canada

ABSTRACT: Nanometer-thick glycine and glycylglycine film growth on Si(111)7×7 at room temperature in ultrahigh vacuum condition and their thermal evolution are investigated by X-ray photoelectron spectroscopy (XPS). In order to understand the XPS result of initial exposure, we also calculate equilibrium geometries and the adsorption energies of plausible glycine and glycylglycine adspecies on model 7×7 surfaces using density functional theory. N 1s spectra reveal three growth stages for both glycine and glycylglycine nanofilms. The first stage involves N−H dissociative adsorption of glycine and N−H and O−H dissociative adsorption of glycylglycine, forming N−Si and O−Si bonds at the interface, respectively. The experimental results are consistent with the most stable glycylglycine adsorption structure involving both the amino and amide N atoms bonded to a Si adatom-restatom pair or an amino N and a carboxyl O atoms bridging two Si adatoms across a dimer wall, in a bidentate configuration. In the second stage, a transitional adlayer grows in the neutral forms of glycine and glycylglycine, binding to their respective interfacial adlayer through hydrogen bonding. For glycine, the presence of head-to-tail N···H−O hydrogen bonding is indicated by a new N 1s feature at 401.4 eV binding energy, between those for neutral amino N at 400.6 eV and zwitterionic N at 402.1 eV. For glycylglycine, the existence of hydrogen bonding can be inferred from the considerable thermal stability of the transitional adlayer (at least to 200 °C). In the final stage, both glycine and glycylglycine grow continuously in the zwitterionic form into thick films. Thermal evolution studies of these as-grown glycine and glycylglycine zwitterionic films on Si(111)7×7 reveal the reverse trend, with the zwitterionic multilayer and transitional adlayer desorbing sequentially and the interfacial adlayer less affected below 250 °C. The glycylglycine film clearly exhibits a higher thermal resistance than the glycine film. The present work demonstrates the vital role of hydrogen bonding in the formation of the transitional adlayer in these important biomolecules. The intermediate bond strength of a hydrogen bond (between those of a covalent bond and the long-range van der Waals interaction) promises new bonding flexibilities for building multifunctional biomolecular structures for biosensor and bioelectronic applications.

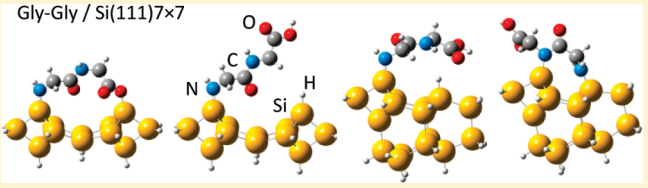

1. INTRODUCTION

Film growth of simple amino acids (e.g., glycine, alanine, and cysteine) on various well-ordered solid surfaces in ultrahigh vacuum has attracted a lot of attention because of their fundamental importance to understanding the interactions of larger biological materials (e.g., proteins and peptides) with solid surfaces. This basic information is prerequisite to building biocatalysts and bioactive devices for sensors and other molecular electronics applications. A number of amino acid molecules have been studied with scanning tunneling microscopy (STM) and found to form self-assembled monolayers or nanoarchitectures on surfaces.[1−4] For example, unidirectional molecular rows of cysteine were grown on Au(110)1 × 2 driven by an adsorbate-induced surface rearrangement[1] and electrostatic interactions between inter- and intra-row neighboring zwitterions.[2] Nanogratings of L-methionine with tunable periodicity could be made on Ag(111) as a result of zwitterionic coupling.[3] The adsorption of glycine on Cu(110) was found to exhibit a sharp "p(3 × 2)g" LEED pattern, which was further resolved into a homochiral and a heterochiral domains by using STM.[4] However, despite the progress in these structural investigations, the film growth process of amino acids from the initial molecular adsorption to multilayer formation is not often well characterized, and the evolution mechanism of molecular structures and chemical bonding properties with increasing film thickness are not well understood.

As the simplest amino acid and peptide respectively, glycine (G) and glycylglycine (GG) are intensely studied as references for more complicated proteins and peptides. Both G and GG can exist in four different forms: the neutral form commonly present in gaseous state, the zwitterionic form found in solids and liquids, and the anionic and cationic forms typically stable in solutions.[5] However, when grown into films on metallic and semiconductor substrates in ultrahigh vacuum, both G and GG may either exist

Received: October 20, 2010
Revised: June 12, 2011
Published: June 13, 2011

in the nonzwitterionic forms or simply dissociate, depending on the nature of the substrates and/or the growth conditions.[6−17] The interactions between different functional groups of G and GG and specific surface sites of the substrate determine their respective forms in the film. A G molecule ($N_aH_2C_\alpha H_2C_cO_nO_hH$) has two functional groups, amino ($-N_aH_2$) and carboxylic acid groups ($-C_cO_nO_hH$), attached to a methylene ($>C_\alpha H_2$) unit, while a GG molecule ($N_aH_2C_{\alpha1}H_2C_pO_pN_pHC_{\alpha2}H_2C_cO_nO_hH$) has an additional amide group ($-C_pO_pN_pH-$) attached to a second methylene unit. In this notation, we have designated the amino and amide N's as N_a and N_p (a for amino and p for peptide-bond related), the methylene C's as $C_{\alpha1}$ and $C_{\alpha2}$, and the amide C (involving the peptide bond) and carboxyl C as C_p and C_c, respectively, and the carbonyl O as O_p and O_n and hydroxyl O as O_h. The Si(111)7×7 surface represents a unique semiconductor surface with 18 directional dangling bonds distributed over six adatoms and three restatoms in each of the faulted and unfaulted triangular half-cells, and one remaining dangling bond shared among the four corner-hole sites.[18] Furthermore, an electron-deficient adatom adjacent to an electron-rich restatom on the Si(111)7×7 surface can act as an electrophile-nucleophile pair (with a separation of 4.6 Å), analogous to the down and up atoms of the Si dimer in the Si(100)2×1 reconstruction (with a typical separation of 2.3 Å).[19,20] The Si surfaces therefore offer interesting bonding sites to explore the selectivity and reactivity of site-specific processes with molecules containing multiple functional groups such as G and GG. In addition to covalent bonding with the Si surface, these biomolecules also offer novel bonding configurations involving intermolecular hydrogen bonding among themselves, potentially introducing new film growth mechanisms.

In the present work, we deposit G and GG on Si(111)7×7 in ultrahigh vacuum, and follow their film growth and subsequent thermal evolution by using X-ray photoelectron spectroscopy (XPS). The adstructures in the early growth stage have also been investigated with ab initio calculations based on the density functional theory (DFT) method. The present results reveal a similar three-stage growth process for both G and GG, with the initial dissociative adsorption followed by an intermediate transition stage involving H-bonding and the final formation of zwitterionic forms in the multilayer film. The thermal evolution of the thick G and GG films displays a reverse trend, with the zwitterionic multilayer and transitional adlayer desorbed sequentially and the interfacial adlayer less affected. The formation of hydrogen bonding in the film growth process can be further exploited for the purpose of Si surface functionalization, for example, by deliberately choosing appropriate linker molecules that will covalently bond to the substrate while providing H-bonding to interact with other target molecules containing the appropriate (multi)functional groups. Given that a hydrogen bond is considerably weaker than a covalent bond yet stronger than a van der Waals bond, this type of hydrogen-bond capable linker molecules may provide a "catch-and-release" mechanism for novel bioapplications.[21]

2. EXPERIMENTAL AND COMPUTATIONAL DETAILS

The experiments were performed in a multichamber ultrahigh vacuum system (Omicron Nanotechnology), with a base pressure better than 5×10^{-11} mbar, described elsewhere.[22] Briefly, the analysis chamber was equipped with a variable-temperature microscope for STM, an XPS spectrometer with a hemispherical electron analyzer, and a monochromatized Al Kα (1486.7 eV) source. The XPS spectra were collected at a typical pass energy of 20 eV, giving an effective instrumental energy resolution of 0.7 eV full width at half-maximum (fwhm) for the Ag $3d_{5/2}$ photoline at 368.3 eV. A Si substrate (2×11 mm^2) was cut from a single-side polished, n-type, As-doped Si(111) wafer (0.3 mm thick), with a resistivity of 0.005 Ω cm (Virginia Semiconductors). The substrate was prepared by outgassing at 400 °C for 12 h, followed by flash-annealing at 1200 °C several times by direct-current heating. After the flashing, large areas of atomically flat terraces of the 7×7 reconstruction could be easily observed by STM and no contamination can be detected by XPS. G (>98.5% purity, Sigma-Aldrich) and GG (>99.5% purity, Sigma-Aldrich), with normal melting points of 182 and ∼220 °C, respectively, were evaporated from separate water-cooled effusion cells at 140 and 170 °C, respectively, onto the clean 7×7 surface held at room temperature in a separate preparation chamber (evacuated by a turbomolecular pump, an ion pump, a cryopump cooled by liquid nitrogen, and a titanium sublimation pump). The corresponding chamber pressure was 1×10^{-8} and 3×10^{-9} mbar during G and GG deposition, respectively. The nature of the G and GG vapors were confirmed by recording their mass spectra [with their respective parent (base) ions of 75 amu (30 amu) and 132 amu (30 amu)][23] with a quadrupole mass spectrometer. Although absolute coverage could in principle be determined from companion STM studies to be reported in our future work,[24] we used the deposition time to indicate the relative exposure and film thickness in the present work. For the film growth experiments, G or GG was deposited sequentially on the same bare Si(111)7×7 substrate, with their corresponding Si 2p, O 1s, N 1s, and C 1s core-level XPS spectra collected after each exposure. All spectra were fitted with mixed Gaussian−Lorentzian lineshapes (70% Gaussian and 30% Lorentzian) with a linear background removal by using the Casa-XPS software. For thick G and GG zwitterionic films, the full width at half maxima (fwhm) for individual components in the C 1s, N 1s, and O 1s spectra are 1.3, 1.5, and 1.5 eV, respectively. For thinner G and GG films where molecules exist in a less homogeneous environment than in thick films, the fwhm of the corresponding components are 0.2−0.3 eV larger. The binding energies are referenced to the Si $2p_{3/2}$ (99.3 eV) of the bulk Si. For the thermal evolution experiments, an as-grown, thick G or GG film was annealed sequentially by resistive heating of the sample holder from 40 up to 250 °C, with the temperature monitored by a thermocouple located close to the sample holder. A relatively long soaking period (600 s) was used to ensure that the reported temperature corresponds to the thermally equilibrated sample due to the different locations between the sample and the thermocouple. The Si 2p, O 1s, N 1s, and C 1s core-level spectra were recorded after each annealing.

The electronic structure calculation was performed by using the Gaussian 03 software.[25] In accordance with the dimer-adatom-stacking fault model of Takayanagi et al.,[18] we used a $Si_{16}H_{18}$ cluster[26] to represent the adatom−restatom sites at the faulted half of the Si(111)7×7 unit cell, with the adatom−restatom distance fixed at 4.57 Å. We also considered adsorption on the center adatom−adatom pair across the dimer wall of the Si(111)7×7 unit cell by using a different $Si_{12}H_{12}$ cluster,[27] with the adatom−adatom distance constrained at 6.65 Å. Equilibrium geometries for the free G or GG molecule, the model cluster of interest and possible adsorbate−substrate configurations (ASCs)

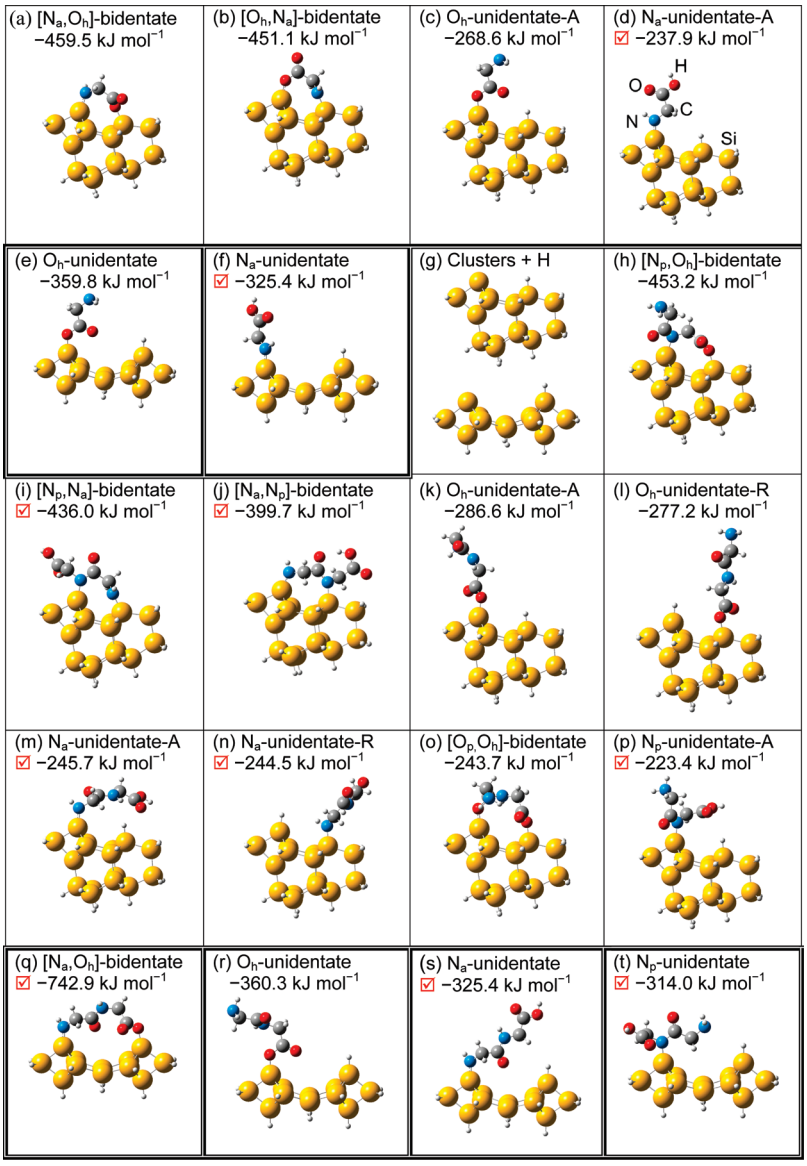

Figure 1. Optimized geometries of adsorbate−substrate configurations (ASCs) and their corresponding adsorption energies of glycine on a $Si_{16}H_{18}$ cluster (a−d) and on a $Si_{12}H_{12}$ cluster (e and f) and of glycylglycine on a $Si_{16}H_{18}$ cluster (h−p) and on a $Si_{12}H_{12}$ cluster (q−t). The optimized geometries of the H adsorbed on $Si_{16}H_{18}$ and $Si_{12}H_{12}$ clusters are shown in (g). The plausible ASCs consistent with the experimental results are marked by red checkmarks.

of G or GG on the model cluster were optimized by using DFT method with the B3LYP hybrid functional.[28−30] Frequency calculations were also performed on the optimized geometries to ensure that no imaginary value was found for the optimized structures that correspond to global minima. The adsorption energy, ΔE, of an ASC was estimated by the difference between the total energies of the product (the ASC itself) and of the reactants, i.e., sum of the total energies of the free molecule (G or GG) and of the model cluster. The adsorption energy of a unidentate adsorption configuration of G or GG could be calculated by using a single model cluster. For the calculation of bidentate adsorption configurations of G or GG, we used three independent (identical) model clusters, with one accounting for the bidentate configuration, the other two (identical) model clusters each for the adsorption of a (dissociated) H atom at the appropriate Si site. All the total energies were obtained without zero point energy correction and no basis set superposition energy correction was made to ΔE. Four different basis sets, including 6-31G(d), 6-31+G(d), 6-31++G(d), and 6-31++G(d,p), have been used. Other than a generally lower total energy found for the larger basis set, no significant difference is observed in the optimized geometry and ΔE of the ASC. In the present work, we only show the computational results obtained for the largest 6-31++G(d,p) basis set.

3. RESULTS AND DISCUSSION

3.1. Computational Chemistry of Adsorption Configurations. Figure 1 shows the equilibrium geometries and the corresponding ΔE values of possible ASCs for G and GG on the model $Si_{16}H_{18}$ and $Si_{12}H_{12}$ surfaces. For G on the $Si_{16}H_{18}$ cluster, both bidentate and unidentate ASCs resulting from,

dx.doi.org/10.1021/jp110055d |J. Phys. Chem. C 2011, 115, 14155–14163

respectively, double and single O_h−H or N_a−H dissociative adsorption have been considered. In particular, the [N_a,O_h]-bidentate ASC (corresponding to amino N_a bonding to the Si adatom and carboxyl O_h bonding to the restatom, Figure 1a) gives a more negative ΔE (−459.5 kJ mol^{-1}) than the [O_h,N_a]-bidentate ASC (corresponding to O_h bonding to the Si adatom and N_a bonding to the restatom, Figure 1b) (−451.1 kJ mol^{-1}), which is consistent with the more basic character of the N_a atom than O_h. The O_h-unidentate-A ASC (corresponding to O_h bonding to the Si adatom, Figure 1c) has a more negative ΔE (−268.6 kJ mol^{-1}) than the N_a-unidentate-A ASC (with N_a bonding to the Si adatom, Figure 1d) (−237.9 kJ mol^{-1}). It should be noted that we use suffixes A and R to indicate adsorption on adatom and restatom, respectively, in the present notation. Given that bonding to the more electrophilic Si adatom is found to give a more stable equilibrium geometry than bonding to the more nucleophilic restatom, we have not shown the corresponding unidentate ASCs for the restatom, which typically exhibit a higher ΔE by 12.5 kJ and 4.5 kJ mol^{-1} for the N_a-unidentate-R and the O_h-unidentate-R products, respectively. For G on the $Si_{12}H_{12}$ cluster, the corresponding unidentate ASCs follow a similar trend as those found on the $Si_{16}H_{18}$ cluster, with the ΔE for O_h-unidentate ASC (Figure 1e, −359.8 kJ mol^{-1}) being more negative than that of N_a-unidentate ASC (Figure 1f, −325.4 kJ mol^{-1}). Our calculation also shows that no stable bidentate ASC involving bridging both adatoms across the dimer wall could be obtained due to the large separation between the two adatoms (6.65 Å) compared to the N_a-to-O_h distance in G (3.7 Å).

It is important to recognize that the present calculation of adsorption energies only gives hints about the feasibility of formation of these ASCs from the thermodynamic perspective. Appropriate consideration of kinetic effects and the underlying formation mechanisms of these ACSs should be included in future work. For the purpose of the present work, we have also considered the formation of adducts of G on the model cluster, which are prerequisite to the formation of these ASCs. Our calculations showed that no stable adducts can be obtained for the O−H dissociative products, including [N_a,O_h]-bidentate, [O_h,N_a]-bidentate, O_h-unidentate-A, and O_h-unidentate ASCs. More detailed discussion of the formation of these adducts is given elsewhere.[31] Despite the more negative ΔEs found for these O−H dissociative products (Figure 1a−c, e), we conclude that the N_a-unidentate-A ASC (Figure 1d) and N_a-unidentate (Figure 1f) are the only plausible products for G on the respective $Si_{16}H_{18}$ and $Si_{12}H_{12}$ model surfaces.

The presence of the amide group (−$C_pO_pN_pH$−) in GG provides additional bidentate and unidentate ASCs on the $Si_{16}H_{18}$ cluster. Indeed, given that the N_a-to-O_h distance in GG (7.31 Å) is considerably larger than the adatom-to-restatom separation (4.57 Å), bonding through the O_p and N_p atoms of the amide group is essential to the formation of bidentate ASCs. In particular, [N_p,O_h]-bidentate (Figure 1h), [N_p,N_a]-bidentate (Figure 1i), and [N_a,N_p]-bidendate ASCs (Figure 1j) on the adatom-restatom pair of the $Si_{16}H_{18}$ surface arise from double N_p−H, and O_h−H or N_a−H dissociation and they provide two dissociated H atoms for Si−H bond formation. These bidentate ASCs give the most negative ΔEs, with magnitude similar to those found for the corresponding bidentate ASCs of G. Additional [O_p,O_h]-bidentate ASC (Figure 1o) involves bonding of the amide O_p and O_h−H dissociative adsorption, giving rise to one dissociated H atom for Si−H bond formation. The corresponding ΔE is found to be notably less negative than those of the other bidendate ASCs and is more similar to those of the O_h-unidentate-A,R (Figure 1k,l), N_a-unidentate-A,R (Figure 1m,n), or N_p-unidentate-A ASC (Figure 1p), arising from a single O_h−H or N_a−H or N_p−H dissociation, respectively. Indeed, the small ΔE difference (33.5 kJ mol^{-1}) found between [O_p,O_h]-bidentate ASC (−243.7 kJ mol^{-1}) and O_h-unidentate-R ASC (−277.2 kJ mol^{-1}) is consistent with the additional energy required for structural rearrangement as a result of the formation of the O_p−Si bond. The N_p-unidentate-A ASC arising from dissociative adsorption of GG through N_p−Si bond formation (Figure 1p) gives less negative ΔE (−223.4 kJ mol^{-1}) than the N_a-unidentate-A ASC (Figure 1m, −245.7 kJ mol^{-1}) through N_a−Si bond formation. Finally, we also obtain other ASCs with higher ΔEs (not shown), including N_p-unidenate-R (−193.1 kJ mol^{-1}), [N_a,O_p]-bidentate (−199.8 kJ mol^{-1}), [N_p,O_h]-bidentate (−198.3 kJ mol^{-1}), and O_p-unidentate-A (−84.1 kJ mol^{-1}). For GG on the $Si_{12}H_{12}$ cluster, the longer N_a-to-O_h distance (7.31 Å) would enable a new [N_a,O_h]-bidentate ASC (Figure 1q) bridging across the two adatoms across the dimer wall. Not surprisingly, the ΔE for this bidentate ASC (−742.9 kJ mol^{-1}) is calculated to be considerably more negative than those of the corresponding unidentate ASCs, including O_h-unidentate (−360.3 kJ mol^{-1}, Figure 1r), N_a-unidentate (−325.4 kJ mol^{-1}, Figure 1s), and N_p-unidentate ASCs (−314.0 kJ mol^{-1}, Figure 1t).

As in the case of G on the $Si_{16}H_{18}$ and $Si_{12}H_{12}$ model surfaces, we also perform an exhaustive search for stable GG adducts as the precursors to the formation of the aforementioned ASCs.[31] These calculations show that stable adducts can be obtained for ASCs involving N−H dissociation and not O−H dissociation of GG on $Si_{16}H_{18}$, including [N_p,N_a]-bidentate (Figure 1i), [N_a,N_p]-bidentate (Figure 1j), N_a-unidentate-A (Figure 1m), N_a-unidentate-R (Figure 1n), and N_p-unidentate-A (Figure 1p). However, stable adduct can be found for [N_a,O_h]-bidentate (Figure 1q) but not O_h-unidentate (Figure 1r) on the $Si_{12}H_{12}$ model surface. We therefore conclude that only ASCs involving N−H dissociation for GG are plausible, with the following relative stability trends based on their ΔE values: [N_a,O_h]-bidentate (ΔE = −742.9 kJ mol^{-1}) > N_a-unidentate (−325.4 kJ mol^{-1}) > N_p-unidentate ASCs (−314.0 kJ mol^{-1}) on $Si_{12}H_{12}$ and [N_p,N_a]-bidendate (−436.0 kJ mol^{-1}) > [N_a,N_p]-bidendate (−399.7 kJ mol^{-1}) > N_a-unidentate-A (−245.7 kJ mol^{-1}) > N_a-unidentate-R (−244.5 kJ mol^{-1}) > N_p-unidentate-A ASCs (−223.4 kJ mol^{-1}) on $Si_{16}H_{18}$.

3.2. X-ray Photoelectron Spectroscopy of G and GG Adsorption. In our recent work,[22] we report detailed XPS spectra of the C 1s, N 1s, and O 1s regions of G as a function of exposure time, as shown in Figure 2. Briefly, G is found to undergo N_a−H dissociative adsorption on Si(111)7×7 upon the initial exposure, as shown by the presence of a prominent N 1s feature at 399.1 eV attributed to the N−Si bond[32−34] at low exposure time <480 s (Figure 2, center). Furthermore, the emergence of a new N 1s feature at 401.4 eV, assigned to N···H−O hydrogen bond, over the 30−480 s exposure range indicates the growth of a transitional adlayer mediated by H-bonding. This observation is consistent with our computational result, which shows that the plausible N_a-unidentate-A ASC on $Si_{16}H_{18}$ (Figure 1d) and N_a-unidentate ASC on $Si_{12}H_{12}$ (Figure 1f) both involve the formation of N−Si bond with the O−H bond intact. Further exposure for over 480 s gives rise to a third N 1s feature at 402.1 eV, which is characteristic of the

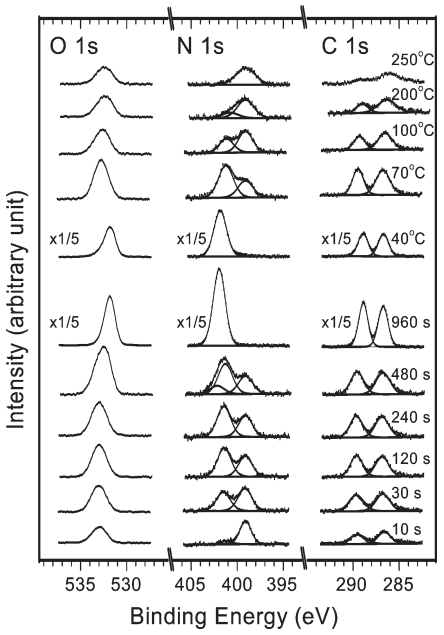

Figure 2. Evolution of C 1s, N 1s, and O 1s spectra of a glycine film deposited on Si(111)7 × 7 as a function of exposure time; and evolution of C 1s, N 1s, and O 1s spectra of a thick as-grown glycine film as a function of annealing temperature.

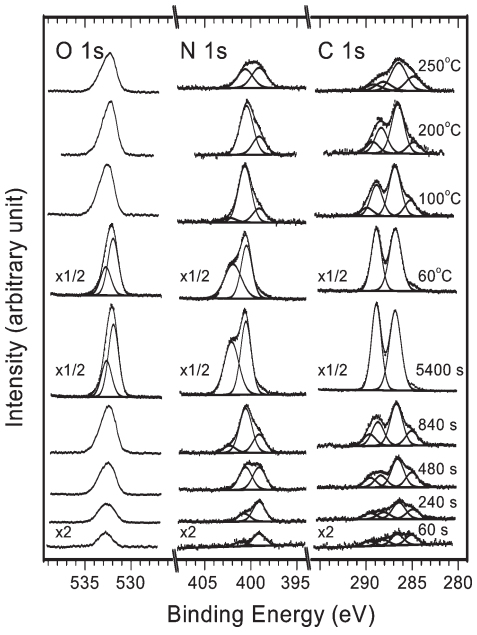

Figure 3. Evolution of C 1s, N 1s, and O 1s spectra of a glycylglycine film deposited on Si(111)7×7 as a function of exposure time; and evolution of C 1s, N 1s, and O 1s spectra of a thick as-grown glycylglycine film as a function of annealing temperature.

protonated amino group (NH_3^+) in the zwitterions.[6,8,35] Based on the saturation intensity ratio of this new hydrogen bond-related N 1s feature at 401.4 eV to the N−Si feature at 399.1 eV (likely corresponding to adsorption of the first or interfacial adlayer), the transition adlayer is estimated to be ∼1.5 times the interfacial adlayer. In the C 1s spectra (Figure 2, right), the two well-defined C 1s peaks at 286.9 and 289.7 eV at shorter exposure times (<960 s) can be assigned to, respectively, methylene (>CH_2) bonded to N and carboxyl C,[8,36] with their intensity ratio close to unity, in good accord with their stoichiometry. For the 960-s exposure, the carboxyl C 1s peak is found to shift by 0.7 eV to a lower binding energy while the methylene C 1s position remains unchanged, which is consistent with the greater delocalization of the negative charge of the carboxylate group in the zwitterionic multilayer. Figure 2 also shows the evolution of the corresponding O 1s spectra of the G film with increasing deposition time (left panel). Below 480 s exposure, the O 1s peak at 533.0 eV is found to be discernibly broader (1.9 eV fwhm) than that at 531.9 eV (1.4 eV fwhm) for 960 s exposure, which can be assigned only to carboxylate O in the zwitterionic multilayer.[6,35] The broad feature is therefore due to multiple components, likely the carbonyl O (C═O) at 532.1−532.9 eV and the hydroxyl O (OH) component at 532.8−534.4 eV.[37−41] Given that the O 1s feature for Si−O bond is usually found at 532.2−532.8 eV,[40,42] the broad O 1s feature is not particularly useful to determine whether O−H dissociative adsorption could occur. For G adsorption, we could however rule out O−H dissociative adsorption from the N 1s spectrum in which no neutral N 1s feature at 400.6 eV is found.

In the present work, we further investigate the observed three-stage growth process by examining the thermal evolution of a thick G film (obtained after the 960-s exposure). Figure 2 also shows the spectral evolution of this G film after sequential annealing to 40, 70, 100, 200, and 250 °C, each for 600 s. After the 40 °C anneal, the C 1s, N 1s, and O 1s spectra remain unchanged in their spectral shapes and peak positions, but considerable intensity reductions (over 50%) are notable, which indicates partial desorption of the thick zwitterionic films after the 40 °C anneal. The remaining zwitterions are totally removed upon further annealing to 70 °C, as indicated by the replacement of the characteristic N 1s feature at 402.1 eV by the N 1s features for N···H−O at 401.4 eV and for N−Si at 399.1 eV and by the shifts of both the O 1s feature (at 531.9 eV) and the carboxyl C 1s feature (at 289.0 eV) to higher binding energy. On the other hand, the hydrogen-bonded transitional adlayer and the covalently bonded interfacial adlayer are hardly affected by further heating at 70 °C. However, continued annealing the sample to 100 °C desorbs about half of the transitional adlayer, as indicated by nearly 50% intensity reduction of the H-bonded N 1s feature at 401.4 eV. The partial desorption of the transitional adlayer leads to a slight intensity increase of the interfacial (N−Si) N 1s feature at 399.1 eV. Annealing to 200 °C almost completely removes the transitional adlayer. The residual N 1s intensity found near 401.0 eV could correspond to the remaining H-bonded N adspecies or thermally dissociated product (e.g., H_2CN)[6] of the transitional and/or interfacial adlayer. An apparent shift of 0.7 eV in the O 1s feature to a lower binding energy (relative to that at 100 °C) suggests the formation of O−Si bond. After the 250 °C anneal, thermal dissociation takes place, as indicated by the more drastic intensity reduction of the two C 1s peaks than those of N 1s and O 1s peaks. Evidently, both the N−Si and O−Si covalent bonding are hardly affected by the anneal at 250 °C. The thermal evolution of the thick G film therefore follows a reverse trend to the film growth.

Figure 3 shows the C 1s, N 1s, and O 1s spectra of a GG film deposited on Si(111)7×7 as a function of exposure time. Evidently, the spectra for a thick film obtained with a 5400-s exposure of GG resemble those of GG powders (not

shown),[35,43] consistent with the zwitterionic form in a thick GG film. The observed spectral similarity also verifies that GG does not dissociate significantly during thermal evaporation in the deposition process. In the zwitterionic form ($N_bH_3^+C_{\alpha1}H_2C_pO_pN_pHC_{\alpha2}H_2C_cO_nO_h^-$), where the two oxygen atoms, O_n and O_h, in the carboxylate group of the zwitterion are equivalent, there are two different types of N species: one in the protonated amino group ($-N_bH_3^+$), and the other in the amide group [$-C_pO_pN_pH-$] containing the peptide bond, which give rise to the N 1s features at 402.2 and 400.6 eV, respectively (Figure 3, center). The observed binding energy positions for these spectral components are consistent with the published results for $-NH_3^+$ (402.0−402.5 eV),[8,35,43−45] as found in G, and for amide in GG powders (400.4 eV)[35,43] and in thymine films (401.0 and 401.2 eV).[46,47] The corresponding energy separation between the N_b 1s and N_p 1s features (1.6 eV) in the zwitterions is found to be nearly the same as that between the N_b 1s and N_a 1s in the amino ($-N_aH_2$) group of the neutral molecular form (1.8 eV) as reported by Clark et al.[35] The N 1s feature of the amide group (N_p) therefore nearly coincides with that of the neutral amino group (N_a), which makes it difficult to differentiate these two features in the present N 1s spectra. The corresponding C 1s spectrum for the 5400-s GG exposure (Figure 3, right) is evidently dominated by two strong features at 286.9 and 288.9 eV with similar intensities, corresponding to the methylene ($C_{\alpha1}$ and $C_{\alpha2}$) and to the carboxyl (C_c) and carbonyl (C_p) species, respectively, in good accord with those found for zwitterionic G films (Figure 2, right) and cysteine film.[36] The very sharp peak at 288.9 eV indicates a very small binding energy difference between the C_p and C_c species. The corresponding O 1s spectrum (Figure 3, left) can be well fitted with two components at 531.9 and 532.7 eV with an intensity ratio of 2:1, with the former attributed to the O_h/O_n in the deprotonated carboxyl group and the latter to the carbonyl O_p. These O 1s binding energies for GG are also in good agreement with those found in G.

The N 1s spectral evolution of GG with increasing exposure time (Figure 3, center) appears to be similar to that found for G (Figure 2, center). In particular, three features at 399.1, 400.6, and 402.2 eV can be identified and assigned to N−Si,[32−34] amide N_p and/or neutral amino N_a, and protonated amino N_b species, respectively. In the initial growth stage (60 s exposure), the spectrum consists of a major component (N−Si) at 399.1 eV and a minor component (amide N_p and/or neutral amino N_a) at 400.6 eV. With further exposure to 240 s, both features increase in intensity with the major feature at 399.1 eV becoming saturated, consistent with the emergence of an interfacial (first) adlayer through N−Si and O−Si bond formation. Because a GG molecule contains one amino N_a and one amide N_p atoms, the presence of a prominent feature at 399.1 eV at low exposure indicates that both the neutral amino and the amide N atoms simultaneously contribute to the N−Si bond formation at the interface. This is because if only one N (either amino or amide) atom is involved in the N−Si bonding while the other N remains unreacted, the N−Si component at 399.1 eV would have equal intensity as the unreacted (amino or amide) N component at 400.6 eV, which is clearly not observed in Figure 3 (center). From a structural point of view, the amino and amide N atoms, with a separation of 3.5 Å, are physically compatible to form covalent bonds with one Si adatom and its nearest restatom neighbor (separated by 4.57 Å) in a bidentate configuration on the Si(111)7×7 surface. This is consistent with our DFT calculation that shows the [N_p,N_a]-bidentate (−436.0 kJ mol^{-1}, Figure 1i), and [N_a,N_p]-bidendate ASCs (−399.7 kJ mol^{-1}, Figure 1j) to be among the most stable ASCs. In addition, the minor feature at 400.6 eV at low exposure may be due to the unreacted amide N_p atom in the [N_a,O_h]-bidentate ASC with the amino N_a atom and hydroxyl O_h atom bridging across the dimer wall (Figure 1q), which has the most negative adsorption energy (−742.9 kJ mol^{-1}). The continued growth of the N_a/N_p 1s feature at 400.6 eV to a feature with almost equal intensity as the N−Si feature at 399.1 eV after 480 s of exposure indicates the addition of GG adlayers in the neutral form. The N_a/N_p 1s feature at 400.6 eV becomes a prominent feature after 840 s exposure, with a weak N 1s feature emerging at 402.2 eV, corresponding to the protonated amino group ($-N_bH_3^+$) in the zwitterions. The emergence of the 402.2 eV feature at the 480-s exposure indicates the on-set of the GG zwitterionic film growth following the formation of a neutral GG transitional adlayer. From the intensities of the spectral features at 400.6 and 399.1 eV obtained at the 840-s exposure (completion of the transitional adlayer) and 240-s exposure (completion of the interfacial adlayer), we estimate the neutral GG transitional adlayer to have a similar thickness as the covalently bonded interfacial adlayer. Like G, the growth of the GG transitional adlayer on the interfacial adlayer is mediated by hydrogen bonding, which is supported by the considerable thermal resistance of the transitional adlayer shown below. Further exposure to 5400 s causes continued increase in the intensities of both the N_b 1s feature at 402.2 eV and the N_p 1s feature at 400.6 eV, indicating the formation of a thick zwitterionic GG film. The N 1s spectra therefore reveal a three-stage, interfacial−transitional−multilayer growth of GG on Si(111)7×7 surface, similar to that found for G growth.

Figure 3 (right) also shows the spectral evolution of the C 1s features of the GG films with increasing exposure time. For exposures other than 5400 s, the C 1s spectra have been fitted with three components at 285.0, 286.6, and 289.6 eV and one component at a position that appears to change with exposure, i.e., 288.1 eV for 60 and 240 s, 288.4 eV for 480 s, and 288.7 eV for 840 s. It has been seen that in the spectral evolution of the C 1s features of the G films (Figure 2, right), the position of the methylene C 1s feature is stable in the three growth stages of G at 286.9 eV, while the position of the carboxyl C 1s feature is also stable at 289.7 eV for the interfacial and transitional adlayers but shifts by 0.7 eV to a lower binding energy in the multilayer. This indicates that the methylene C 1s feature is hardly affected by the change of the G forms, whereas the carboxyl C 1s feature changes considerably when the carboxylic acid group (COOH) deprotonates to carboxylate (COO^-), as a result of charge delocalization in the carboxylate. In a neutral GG molecule ($N_aH_2C_{\alpha1}H_2C_pO_pN_pHC_{\alpha2}H_2C_cO_nO_hH$), there are two methylene $C_{\alpha1}$ and $C_{\alpha2}$, one amide C_p, and one carboxyl C_c atoms, the binding energies of which are expected to increase in the sequence of ($C_{\alpha1}$, $C_{\alpha2}$) < C_p < C_c from a simple consideration of the electronegativity of their nearest neighbors. Based on the magnitude and constancy of the binding energies of the fitted components, we therefore assign the features at 286.6, 288.1−288.7, and 289.6 eV, respectively, to the two methylene $C_{\alpha1}$ and $C_{\alpha2}$ atoms, amide C_p, and carboxyl C_c. The gradual increase of the amide C_p 1s binding energy with increasing exposure is in accord with the binding energy increase of the N_p 1s from 399.1 eV for the interfacial adlayer to 400.6 eV for the transitional adlayer as a result of electron delocalization in the peptide bond.

In particular, the largely negatively charged N_p atoms at the interfacial adlayer lead to a correspondingly larger electron density in the C_p atoms and therefore a lower binding energy. The C_p 1s binding energy (288.7 eV) for the 840-s exposure is in agreement with that (288.9 eV) of a peptide bond in thymine.[47] The intensity of the methylene C 1s feature is close to the sum of that of the carboxyl and amide C 1s features, in agreement with the C stoichiometry of GG. With further increase in exposure, formation of GG zwitterions, as in the case of G, gives rise to a considerable shift (0.7 eV) of the carboxyl C_c 1s feature to the lower binding energy side and eventually merging with the amide C_p 1s feature to form a sharp peak at 288.9 eV in the 5400-s thick film. Finally, the component at 285.0 eV is located at a 1.6 eV lower in binding energy than the methylene C and seems to be unrelated to GG. Because such a low binding energy could only result from formation of C−Si bond following C−H bond cleavage and dissociation other than N−H or O−H bond upon GG adsorption is unlikely, we attribute this feature at 285.0 eV to residual hydrocarbon species likely arising from thermal evaporation of GG during the exposure process. A similar hydrocarbon residual peak at 285 eV has also been reported for thermally evaporated dipeptide and tripeptide films on Au(110)[48] and thick films of DNA base groups on H-terminated Si(111) under ultrahigh vacuum.[49] Figure 3 (left) also shows the corresponding O 1s spectra of the GG film with increasing deposition time. Like the G film, the O 1s spectra are dominated by a broad feature at 532.7 eV, with its width (2.0 eV fwhm) for exposures lower than 840 s discernibly larger than that for the 5400-s exposure (1.4 eV fwhm). We have previously assigned the O 1s feature for the 5400-s exposure to the deprotonated carboxylate O_n/O_h component (at 531.9 eV) and the carbonyl O_p component (at 532.7 eV) in the zwitterionic multilayer. The broad feature found at lower exposures can be due to a combination of carbonyl O at 532.1−532.9 eV and hydroxyl O component at 532.8−534.4 eV[37−41] and is not very useful for revealing whether O−H dissociative adsorption could occur.

Thermal evolution of the thick GG film with the 5400-s exposure on Si(111)7×7 was studied by recording the C 1s, N 1s, and O 1s spectra after sequentially annealing to 60, 100, 200, and 250 °C, each for 600 s (Figure 3). After the 60 °C anneal, the C 1s, N 1s and O 1s spectral profiles remain largely unchanged, except for a ∼20% reduction in their intensities, which indicates desorption of a small amount of GG zwitterions. However, annealing at 100 °C almost totally removes the GG zwitterions, as indicated by the dramatic near-complete reduction of the N 1s feature (of $-N_bH_3^+$) at 402.2 eV (Figure 3, center). The resulting C 1s, N 1s, and O 1s spectra appear similar to those of the film after 840-s exposure, which suggests that the transitional and interfacial adlayers remain stable to 100 °C, in contrast to the G transitional adlayers, half of which desorb at 100 °C (Figure 2). Surprisingly, further annealing to 200 °C does not appear to have a significant effect on the spectra, indicating that most of the transitional adlayer still remains intact at 200 °C. This relatively high thermal stability of the transitional adlayer is consistent with the presence of additional H−bonding interactions in the GG transitional adlayer. The three functional groups in a GG molecule facilitate H−bonding formation among them. However, the absence of the N 1s feature at 401.4 eV suggests that the O_h−H···N_a hydrogen bonding in the head-to-tail configuration does not occur, in contrast to that found in the G transitional adlayers. This may be due to an unfavorable orientation of the O_h−H moiety in the interfacial adlayer for hydrogen bonding with the incoming GG molecules and/or availability of other stronger hydrogen bonding. Instead, $N_{a\ or\ p}$−H···O_n=C_c and $N_{a\ or\ p}$−H···O_p=C_p H-bonding between an amino or amide group in the transitional adlayer and the carbonyl O in the interfacial adlayer, and/or O_h−H···O_n=C_c and O_h−H···O_p=C_p H-bonding between a hydroxyl O in the transitional adlayer and a carbonyl O in the interfacial adlayer may account for the relatively high thermal stability of the transitional adlayer. Indeed, extensive intermolecular amide−amide H−bonding has been reported to cause a higher onset temperature (by 125 °C) of thermal desorption of amide-containing alkanethiol self-assembled monolayers on Au.[50,51] Unfortunately, the inherently large linewidths of the O 1s features do not allow definitive identification of the types of the H−bonds. After the 250 °C anneal, the spectra become similar to those for the as-deposited film obtained after 480 s of exposure. Considerable reduction in the intensity of the N_a/N_p 1s feature at 400.6 eV (Figure 3, center) is observed, which indicates that nearly half of the transitional adlayer has been removed. These annealing experiments show that the GG transitional adlayer is more strongly bonded than the G transitional adlayer, which almost completely desorbs at 200 °C. Like the G film, the thermal evolution of the thick GG film also follows a similar reverse growth process.

3.3. Comparison of XPS Results with the Calculations. Having presented both the plausible ASCs and XPS results, we are able to relate the most favorable ASCs, i.e., those having the most negative adsorption energies, to the XPS results of the interfacial adlayer, as represented by the 10-s G and 60-s GG films. The N 1s spectrum for the 10-s G film (Figure 2) clearly shows that G molecules bond to the Si(111)7×7 surface with covalent N−Si bonding after N−H bond cleavage. On the other hand, we notice that the corresponding N_a-unidentate-A configuration (Figure 1d) does not have the most negative adsorption energy. In a typical calculation of reaction pathways between a molecule and model surface, a stable adduct is prerequisite to the formation of a reaction product. A transition state with an energy barrier may sometimes exist between the stable adduct and the final reaction product. Without a stable adduct, the corresponding reaction pathway may not be initiated. Our calculations show that a stable adduct can form for the N−H dissociative product, but not for the O−H dissociative product.[31] The dominance of the N−Si feature in the N 1s spectrum for the 60-s GG film (Figure 3) indicates that both N atoms in the GG molecule bond to Si, which is consistent with the calculated [N_p,N_a]-bidentate (Figure 1i) and [N_a,N_p]-bidentate ASCs (Figure 1j), the adsorption energies of which are among the most negative ones on the $Si_{16}H_{18}$ model surface. On the other hand, the clearly discernible N 1s feature at 400.6 eV for the 60-s GG film (Figure 3) can be attributed to the N_p in the [N_a,O_h]-bidentate ASC (Figure 1q), which has the most negative adsorption energy on the $Si_{12}H_{12}$ model surface.

4. CONCLUSION

We have investigated the growth of G and GG films on Si(111)7×7 at room temperature and their thermal evolution in ultrahigh vacuum by XPS. The equilibrium geometries and their corresponding adsorption energies of plausible adstructures for G and GG on an adatom-restatom pair (of a $Si_{16}H_{18}$ cluster) and on a center-adatom-to-center-adatom pair (of a $Si_{12}H_{12}$ cluster) were calculated by using the DFT/B3LYP method. From the spectral changes of the N 1s features with increasing

exposure, three growth stages can be identified for G and GG films, and they correspond to the sequential formation of the covalently bonded interfacial adlayer, the hydrogen-bond-mediated transitional adlayer, and the zwitterionic multilayer. In the initial growth stage, G molecules adsorb on the 7×7 surface in a unidentate configuration by N−H bond dissociation, whereas GG molecules adsorb in bidentate configurations via bond dissociation of N_a−H and N_p−H bonds at an adatom−restatom site or of N_a−H and O_h−H bonds at a center-adatom−center-adatom dimer-wall site. Our XPS results are consistent with the three most stable, calculated [N_a,N_p]-, [N_p, N_a]-, and [N_a,O_h]-bidentate ASCs for a GG molecule. In the intermediate growth stage, formation of a transitional adlayer appears to be mediated by hydrogen bonding. For G, a head-to-tail $N_a\cdots H-O_h$ hydrogen-bond configuration is supported by the presence of a new N 1s feature at 401.4 eV, i.e. an intermediate binding energy between those of N^0 (400.6 eV) and N^{1+} (402.1 eV). On the other hand, the existence of hydrogen bonding for GG can be inferred from the relatively high thermal stability of the transitional adlayer (up to 200 °C), as observed from the XPS spectral changes upon sequential annealing. The transitional adlayers of G and GG are estimated to be one to two times as thick as their respective interfacial adlayers. In the final growth stage, G and GG grow continuously into multilayers in the zwitterionic form, consistent with it being their most stable solid forms. Thermal evolution studies of these as-grown thick G and GG films on Si(111)7×7 reveal a reverse growth process, with the zwitterionic multilayer desorbed before the transitional adlayer, and the interfacial adlayer remaining unaffected at least to 200 and 250 °C, respectively. The present work illustrates that hydrogen bonding plays a key role in the formation of the transitional adlayer in these important biomolecules. Given the intermediate bond strength of a hydrogen bond (between a covalent bond and the long-range van der Waals interaction), this hydrogen-bond mediated transitional adlayer offers new bonding flexibilities for building multifunctional biomolecular structures appropriate for biosensor and bioelectronic applications.

■ ACKNOWLEDGMENT

The work was supported by the Natural Sciences and Engineering Research Council of Canada.

■ REFERENCES

(1) Kuhnle, A.; Molina, L. M.; Linderoth, T. R.; Hammer, B.; Besenbacher, F. *Phys. Rev. Lett.* **2004**, *93*, 086101.
(2) Cossaro, A.; Terreni, S.; Cavalleri, O.; Prato, M.; Cvetko, D.; Morgante, A.; Floreano, L.; Canepa, M. *Langmuir* **2006**, *22*, 11193.
(3) Schiffrin, A.; Riemann, A.; Auwarter, W.; Pennec, Y.; Weber-Bargioni, A.; Cvetko, D.; Cossaro, A.; Morgante, A.; Barth, J. V. *Proc. Natl. Acad. Sci. U.S.A.* **2007**, *104*, 5279.
(4) Chen, Q.; Frankel, D. J.; Richardson, N. V. *Surf. Sci.* **2002**, *497*, 37.
(5) Nyberg, M.; Hasselstrom, J.; Karis, O.; Wassdahl, N.; Weinelt, M.; Nilsson, A.; Pettersson, L. G. M. *J. Chem. Phys.* **2000**, *112*, 5420.
(6) Lofgren, P.; Krozer, A.; Lausmaa, J.; Kasemo, B. *Surf. Sci.* **1997**, *370*, 277.
(7) Tzvetkov, G.; Mamsey, M. G.; Netzer, F. P. *Surf. Sci.* **2003**, *526*, 383.
(8) Tzvetkov, G.; Koller, G.; Zubavichus, Y.; Fuchs, O.; Casu, M. B.; Heske, C.; Umbach, E.; Grunze, M.; Mamsey, M. G.; Netzer, F. P. *Langmuir* **2004**, *20*, 10551.
(9) Barlow, S. M.; Kitching, K. J.; Haq, S.; Richardson, N. V. *Surf. Sci.* **1998**, *401*, 322.
(10) Hasselstrom, J.; Karis, O.; Weinelt, M.; Wassdahl, N.; Nilsson, A.; Nyberg, M.; Pettersson, L. G. M.; Samant, M. G.; Stohr, J. *Surf. Sci.* **1998**, *407*, 221.
(11) Feyer, V.; Plekan, O.; Tsud, N.; Lyamayev, V.; Chab, V.; Matolin, V.; Prince, K. C.; Carravetta, V. *J. Phys. Chem. C* **2010**, *114*, 10922.
(12) Huang, J. Y.; Ning, Y. S.; Yong, K. S.; Cai, Y. H.; Tang, H. H.; Shao, Y. X.; Alshahateet, S. F.; Sun, Y. M.; Xu, G. Q. *Langmuir* **2007**, *23*, 6218.
(13) Zhao, X. Y.; Rodriguez, J. *Surf. Sci.* **2006**, *600*, 2113.
(14) Gao, F.; Li, Z. J.; Wang, Y. L.; Burkholder, L.; Tysoe, W. T. *J. Phys. Chem. C* **2007**, *111*, 9981.
(15) Wu, C. R.; Nilsson, J. O.; Salaneck, W. R. *Phys. Scr.* **1987**, *35*, 586.
(16) Lange, W.; Jirikowsky, M.; Benninghoven, A. *Surf. Sci.* **1984**, *136*, 419.
(17) Holtkamp, D.; Jirikowsky, M.; Kempken, M.; Benninghoven, A. *J. Vac. Sci. Technol. A* **1985**, *3*, 1394.
(18) Takayanagi, K.; Tanishiro, Y.; Takahashi, S. *J. Vac. Sci. Technol. A* **1985**, *3*, 1502.
(19) Tao, F.; Xu, G. Q. *Acc. Chem. Res.* **2004**, *37*, 882.
(20) Tao, F.; Lai, Y. H.; Xu, G. Q. *Langmuir* **2004**, *20*, 366.
(21) Zhang, L.; Chatterjee, A.; Leung, K. T. *J. Phys. Chem. Lett.* **2010**, *1*, 3385.
(22) Zhang, L.; Chatterjee, A.; Ebrahimi, M.; Leung, K. T. *J. Chem. Phys.* **2009**, *130*, 121103.
(23) NIST Chemistry WebBook, http://webbook.nist.gov/chemistry.
(24) Chatterjee A.; Zhang L.; Leung K. T. to be published.
(25) Frisch, M. J.; et al. *Gaussian 03*; Gaussian, Inc.: Wallingford, CT, 2005.
(26) Bournel, F.; Carniato, S.; Dufour, G.; Gallet, J. J.; Ilakovac, V.; Rangan, S.; Rochet, F. *Phys. Rev. B* **2006**, *73*, 125345.
(27) Lee, H. S.; Choi, C. H. *Theor. Chem. Acc.* **2008**, *120*, 79.
(28) Kohn, W.; Sham, L. *J. Phys. Rev.* **1965**, *140*, A1133.
(29) Becke, A. D. *J. Chem. Phys.* **1993**, *98*, 5648.
(30) Lee, C.; Yang, W.; Parr, R. G. *Phys. Rev. B* **1989**, *37*, 785.
(31) Chatterjee, A.; Zhang, L.; Leung, K. T. *Chem. Phys. Lett.* **2011**, *508*, 219.
(32) Cao, X. P.; Hamers, R. J. *J. Vac. Sci. Technol. B* **2002**, *20*, 1614.
(33) Cao, X. P.; Hamers, R. J. *Surf. Sci.* **2003**, *523*, 241.
(34) Cao, X. P.; Hamers, R. J. *J. Am. Chem. Soc.* **2001**, *123*, 10988.
(35) Clark, D. T.; Peeling, J.; Colling, L. *Biochim. Biophys. Acta* **1976**, *453*, 533.
(36) Gonella, G.; Terreni, S.; Cvetko, D.; Cossaro, A.; Mattera, L.; Cavalleri, O.; Rolandi, R.; Morgante, A.; Floreano, L.; Canepa, M. *J. Phys. Chem. B* **2005**, *109*, 18003.
(37) Briggs, D.; Beamson, G. *Anal. Chem.* **1993**, *65*, 1517.
(38) Lopez, G. P.; Castner, D. G.; Ratner, B. D. *Surf. Interface Anal.* **1991**, *17*, 267.
(39) Buchwalter, L. P.; Czornyj, G. *J. Vac. Sci. Technol. A* **1990**, *8*, 781.
(40) Tang, H. H.; Cai, Y. H.; Ning, Y. S.; Lai, Y. H.; Xu, G. Q. *Surf. Sci.* **2007**, *601*, 3293.
(41) Huang, J. Y.; Shao, Y. X.; Huang, H. G.; Cai, Y. H.; Ning, Y. S.; Tang, H. H.; Liu, Q. P.; Alshahateet, S. F.; Sun, Y. M.; Xu, G. Q. *J. Phys. Chem. B* **2005**, *109*, 19831.
(42) Tang, H. H.; Dai, Y. J.; Shao, Y. X.; Ning, Y. S.; Huang, J. Y.; Lai, Y. H.; Peng, B.; Huang, W.; Xu, G. Q. *Surf. Sci.* **2008**, *602*, 2647.
(43) Chatterjee, A.; Zhao, L. Y.; Zhang, L.; Pradhan, D.; Zhou, X. J.; Leung, K. T. *J. Chem. Phys.* **2008**, *129*, 105104.
(44) Uvdal, K.; Bodo, P.; His, A.; Liedberg, B.; Salaneck, W. R. *J. Colloid Interface Sci.* **1990**, *140*, 207.
(45) Iucci, G.; Battocchio, C.; Dettin, M.; Gambaretto, R.; Di Bello, C.; Borgatti, F.; Carravetta, V.; Monti, S.; Polzonetti, G. *Surf. Sci.* **2007**, *601*, 3843.
(46) Petrovykh, D. Y.; Kimura-Suda, H.; Whitman, L. J.; Tarlov, M. J. *J. Am. Chem. Soc.* **2003**, *125*, 5219.

(47) Haug, A.; Schweizer, S.; Latteyer, F.; Casu, M. B.; Peisert, H.; Ochsenfeld, C.; Chasse, T. *Chem. Phys. Chem.* **2008**, *9*, 740.
(48) Vallee, A.; Humblot, V.; Methivier, C.; Pradier, C. M. *J. Phys. Chem. C* **2009**, *113*, 9336.
(49) Seifert, S.; Gavrila, G. N.; Zahn, D. R. T.; Braun, W. *Surf. Sci.* **2007**, *601*, 2291.
(50) Clegg, R. S.; Reed, S. M.; Hutchison, J. E. *J. Am. Chem. Soc.* **1998**, *120*, 2486.
(51) Lewis, P. A.; Smith, R. K.; Kelly, K. F.; Bumm, L. A.; Reed, S. M.; Clegg, R. S.; Gunderson, J. D.; Hutchison, J. E.; Weiss, P. S. *J. Phys. Chem. B* **2001**, *105*, 10630.